CORA Cork Open Research Archive
Cartlann Taighde Oscailte Chorcaí

Title	Compositional characterisation of metallurgical grade silicon and porous silicon nanosponge particles
Authors	Chadwick, Edward G.;Mogili, N. V. V.;O'Dwyer, Colm;Moore, Jimmy D.;Fletcher, John S.;Laffir, Fathima;Armstrong, Gordon;Tanner, David A.
Publication date	2013-08-02
Original Citation	Chadwick, E. G., Mogili, N. V. V., O'Dwyer, C., Moore, J. D., Fletcher, J. S., Laffir, F., Armstrong, G. and Tanner, D. A. (2013) 'Compositional characterisation of metallurgical grade silicon and porous silicon nanosponge particles', RSC Advances, 3(42), pp. 19393-19402. doi: 10.1039/C3RA42205D
Type of publication	Article (peer-reviewed)
Link to publisher's version	http://pubs.rsc.org/en/content/articlepdf/2013/ra/c3ra42205d - 10.1039/C3RA42205D
Rights	© Royal Society of Chemistry 2013
Download date	2026-11-07 07:45:02
Item downloaded from	https://hdl.handle.net/10468/6134

UCC
University College Cork, Ireland
Coláiste na hOllscoile Corcaigh

View Article Online
View Journal

RSC Advances

Accepted Manuscript

This article can be cited before page numbers have been issued, to do this please use: E. G. Chadwick, N. V. Mogili, C. O'Dwyer, J. D. Moore, J. Fletcher, F. R. Laffir, G. Armstrong and D. A. Tanner, *RSC Adv.*, 2013, DOI: 10.1039/C3RA42205D.



This is an *Accepted Manuscript*, which has been through the RSC Publishing peer review process and has been accepted for publication.

Accepted Manuscripts are published online shortly after acceptance, which is prior to technical editing, formatting and proof reading. This free service from RSC Publishing allows authors to make their results available to the community, in citable form, before publication of the edited article. This *Accepted Manuscript* will be replaced by the edited and formatted *Advance Article* as soon as this is available.

To cite this manuscript please use its permanent Digital Object Identifier (DOI®), which is identical for all formats of publication.

More information about *Accepted Manuscripts* can be found in the **Information for Authors**.

Please note that technical editing may introduce minor changes to the text and/or graphics contained in the manuscript submitted by the author(s) which may alter content, and that the standard **Terms & Conditions** and the **ethical guidelines** that apply to the journal are still applicable. In no event shall the RSC be held responsible for any errors or omissions in these *Accepted Manuscript* manuscripts or any consequences arising from the use of any information contained in them.

View Article Online
DOI: 10.1039/C3RA42205D

COMPOSITIONAL CHARACTERISATION OF METALLURGICAL GRADE SILICON AND POROUS SILCION NANOSPONGE PARTICLES, Chadwick *et al.*

Figures

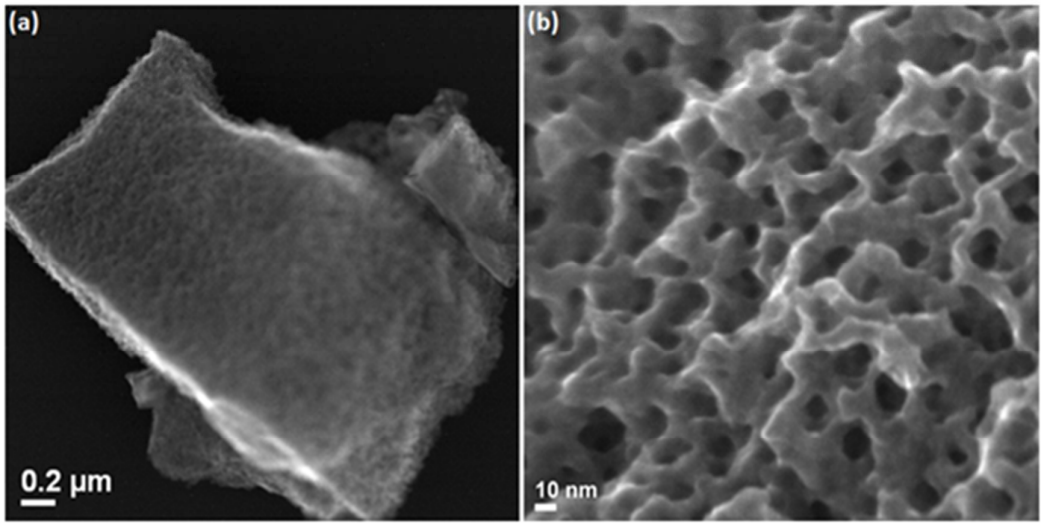


Figure 1 (a) SEI micrograph of sample 2E-100 oriented in [3 4 0] zone axis (b) Corresponding higher magnified image clearly showing porous nature of the particle

Published on 02 August 2013. Downloaded by University College Cork on 07/08/2013 15:02:52.

RSC Advances Accepted Manuscript

View Article Online
DOI: 10.1039/C3RA42205D

Published on 02 August 2013. Downloaded by University College Cork on 07/08/2013 15:02:52.

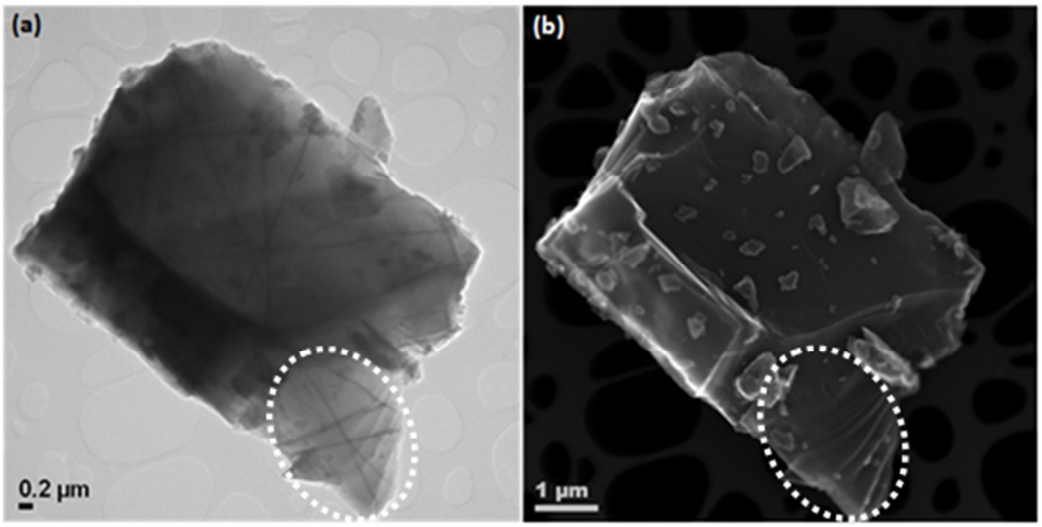


Figure 2 a) Convergent Beam Imaging (CBIM) micrograph of [340] oriented unetched Si particle exhibiting both real and reciprocal space information b) Corresponding Secondary Electron Image (SEI) of unetched Si particle illustrating the surface morphology of the crystal

RSC Advances Accepted Manuscript

View Article Online
DOI: 10.1039/C3RA42205D

Published on 02 August 2013. Downloaded by University College Cork on 07/08/2013 15:02:52.

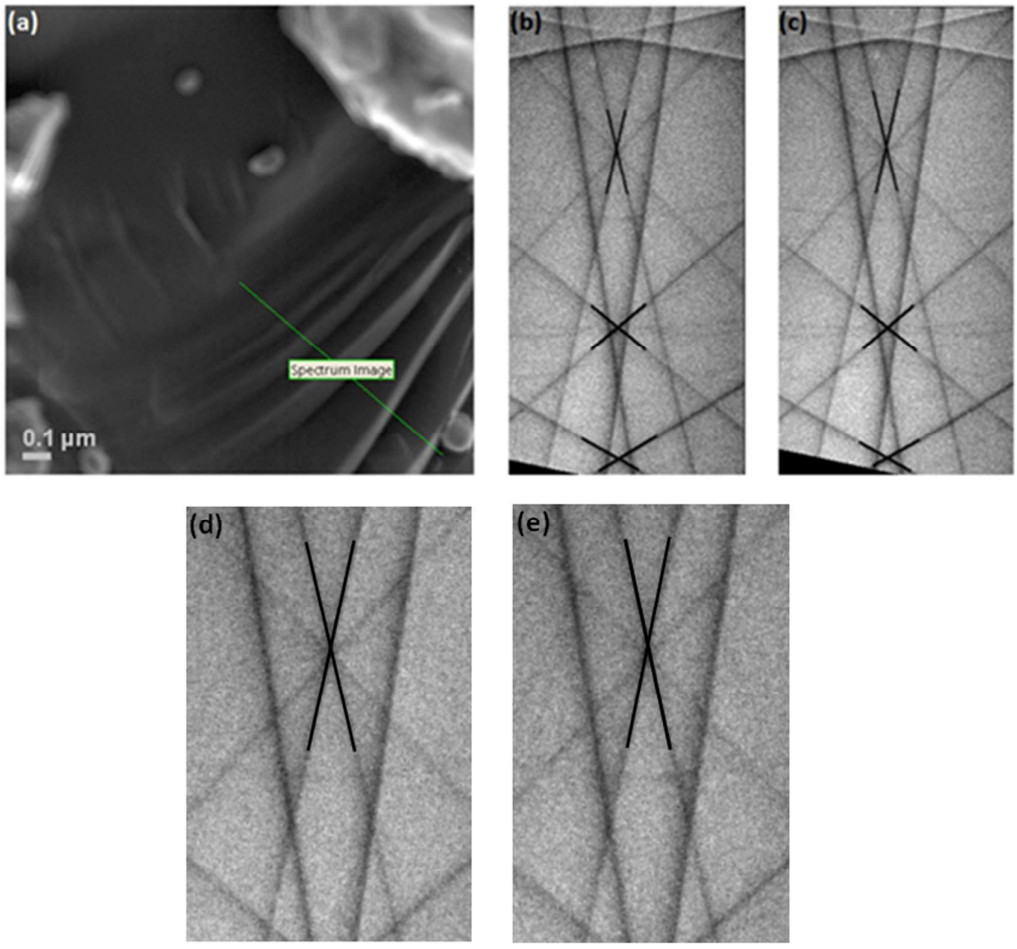


Figure 3a) SEI image of a 2E-Bulk particle indicating the spectrum image line where sequential CBED patterns are collected b), c) Two [340] CBED patterns taken from spectrum image and HOLZ lines intersection points which are very sensitive for lattice changes are highlighted d), e) Enlarged region of [340] HOLZ lines showing that there is no shift / change in intersection point.

RSC Advances Accepted Manuscript

View Article Online
DOI: 10.1039/C3RA42205D

Published on 02 August 2013. Downloaded by University College Cork on 07/08/2013 15:02:52.

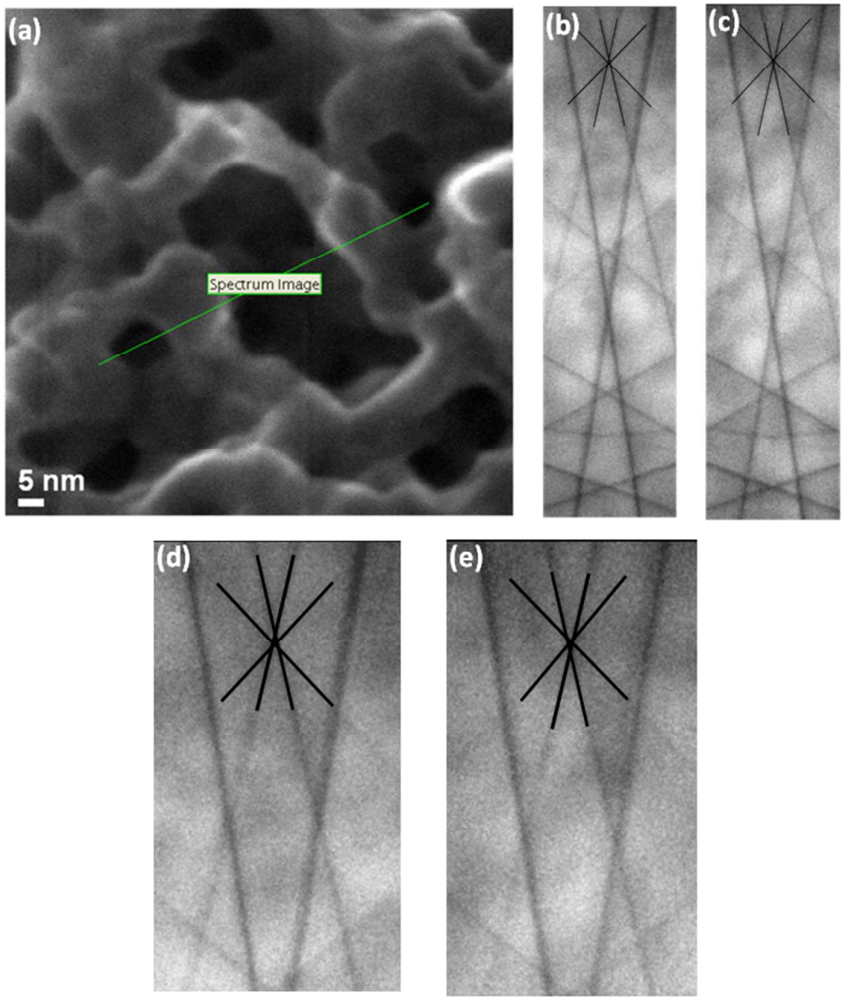


Figure 4a) High resolution SEI micrograph of sample 2E-100 PS sample showing spectrum imaging location of one particular pore b), c) Two [340] CBED patterns collected from spectrum image showing the shift of HOLZ line position d), e) Enlarged region of [340] HOLZ lines clearly showing shift in the position of intersection point. (Reader is advised to go through the supplementary video file in order to visualise how the HOLZ lines move in the spectrum imaging patterns)

RSC Advances Accepted Manuscript

View Article Online
DOI: 10.1039/C3RA42205D

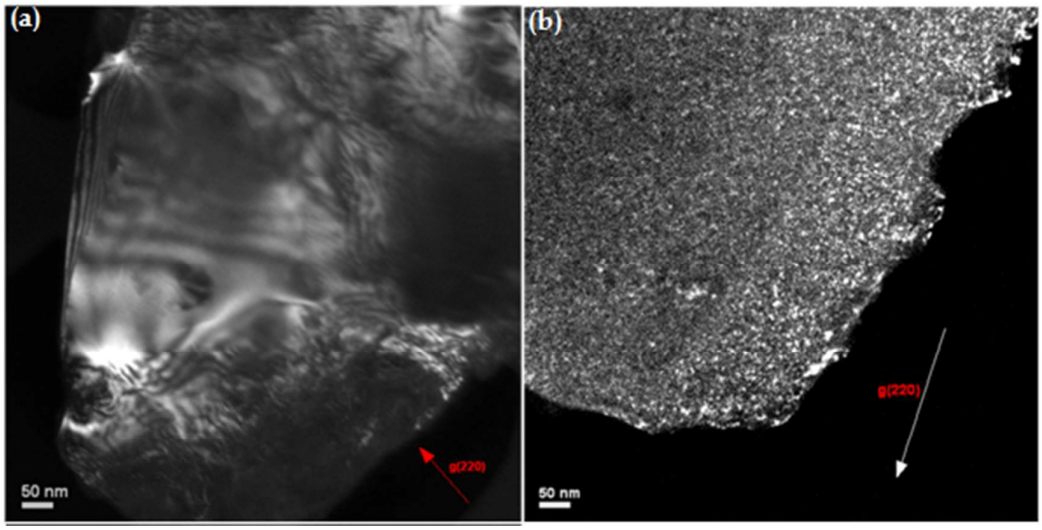


Figure 5 (a) Typical <220> dark field images of sample 2E-Bulk Si particle and (b) sample 2E-100 PS particle

Published on 02 August 2013. Downloaded by University College Cork on 07/08/2013 15:02:52.

RSC Advances Accepted Manuscript

View Article Online
DOI: 10.1039/C3RA42205D

Published on 02 August 2013. Downloaded by University College Cork on 07/08/2013 15:02:52.

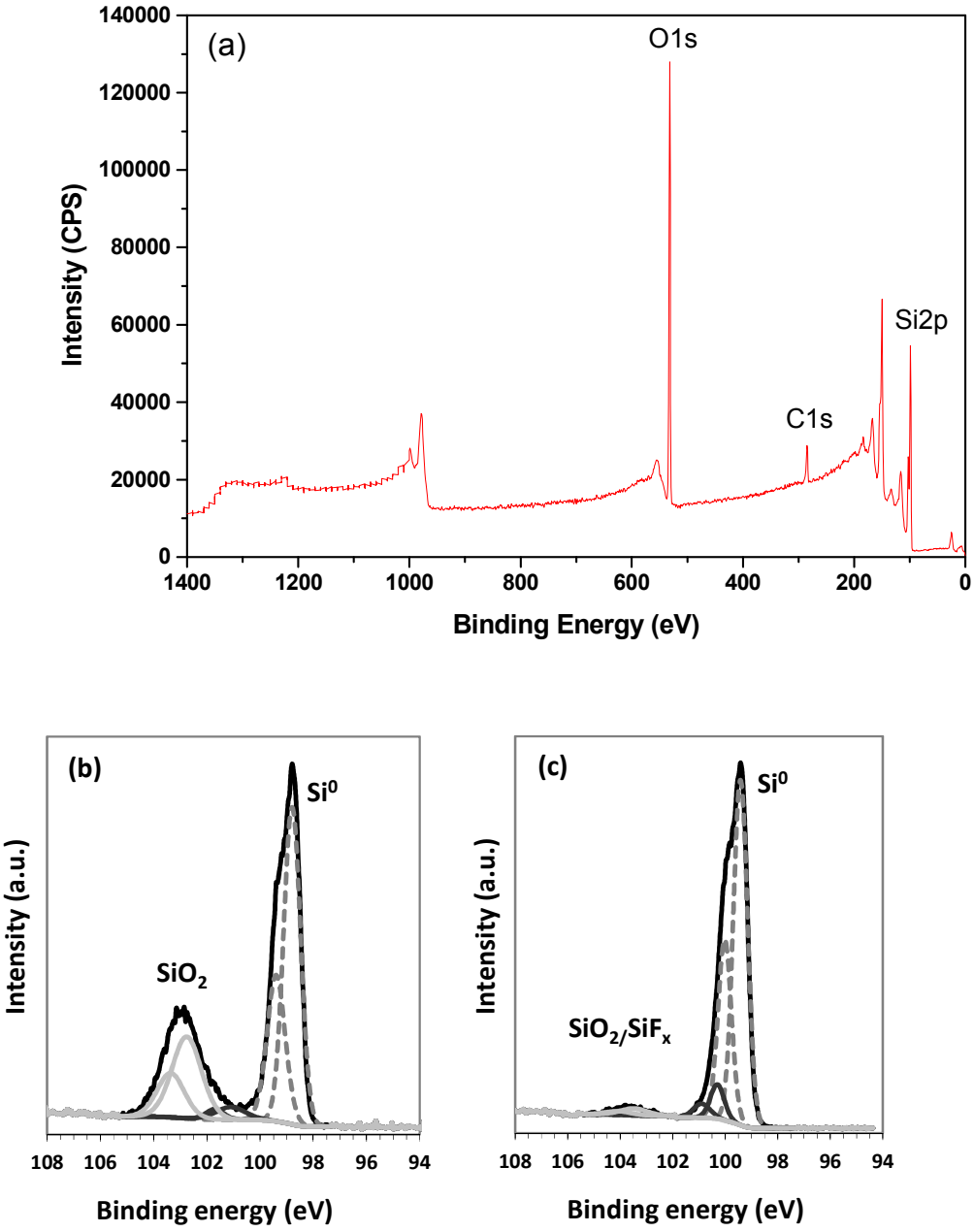


Figure 6 a) XPS analysis of sample 2E-Bulk; b) and c) High resolution Si 2p spectra of 2E-Bulk and 2E-60 respectively.

RSC Advances Accepted Manuscript

View Article Online
DOI: 10.1039/C3RA42205D

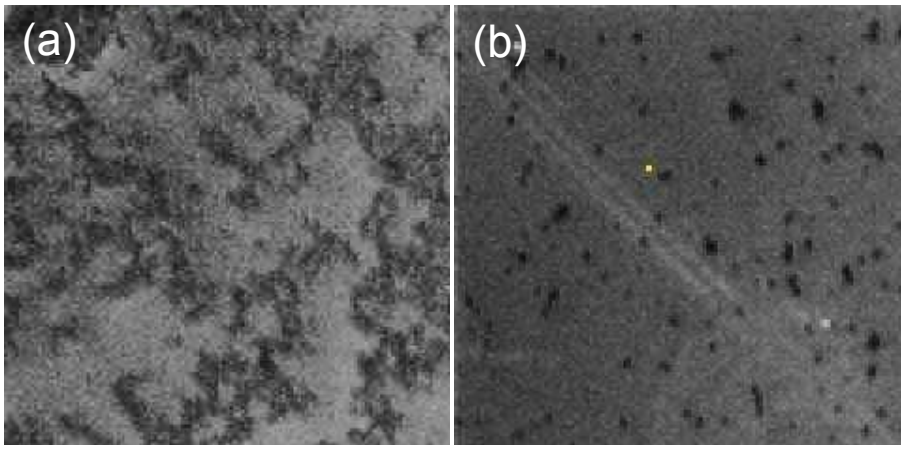


Figure 7 Total ion images (500 × 500 μm^2) of (a) 2E-Bulk sample (b) 2E-100 particles.

Published on 02 August 2013. Downloaded by University College Cork on 07/08/2013 15:02:52.

RSC Advances Accepted Manuscript

View Article Online
DOI: 10.1039/C3RA42205D

Published on 02 August 2013. Downloaded by University College Cork on 07/08/2013 15:02:52.

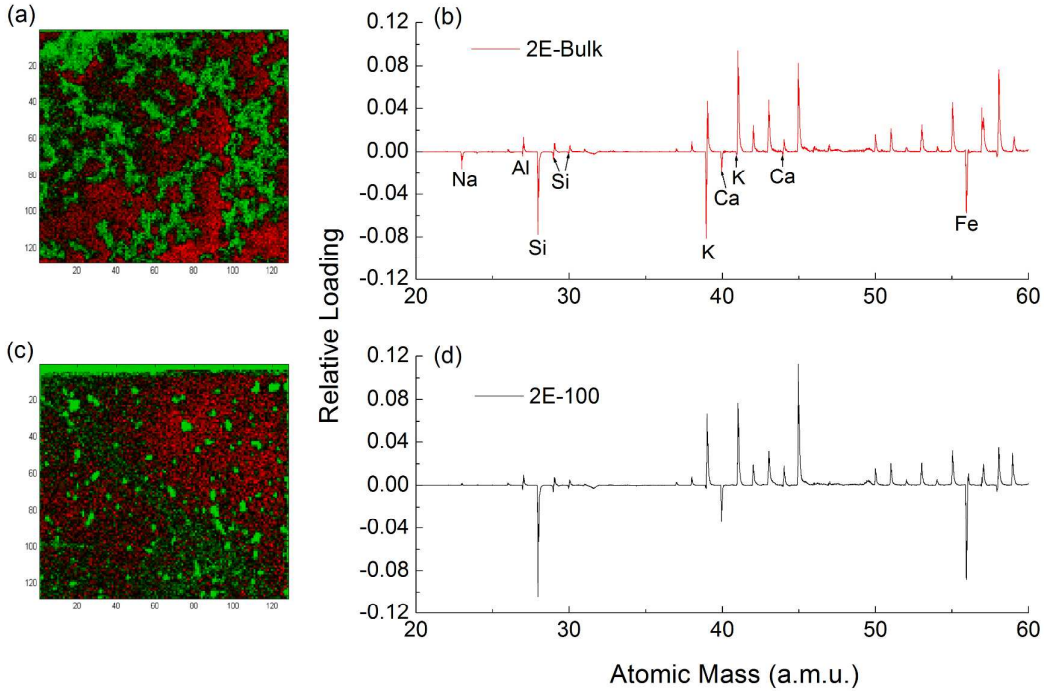


Figure 8 (a, b) Scores image and the corresponding TOF-SIMS loading spectrum from PC2 of the 2E-Bulk Si particles and (c, d) from PC3 of the etched 2E-100 Si particles.

RSC Advances Accepted Manuscript

View Article Online
DOI: 10.1039/C3RA42205D

Published on 02 August 2013. Downloaded by University College Cork on 07/08/2013 15:02:52.

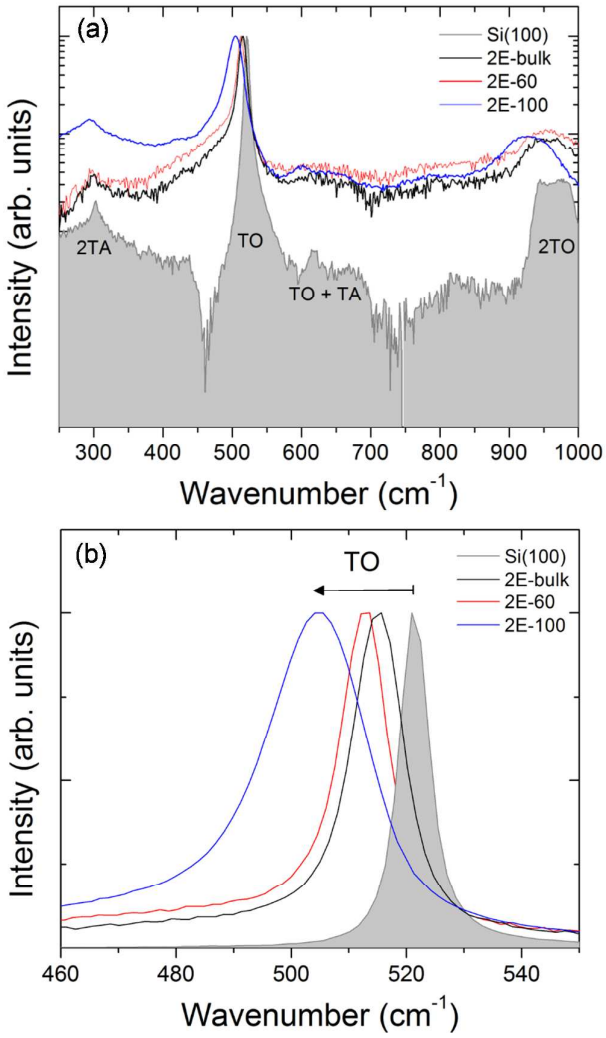


Figure 9 (a) Micro-Raman Spectrum of PS samples 2E-100, 2E-60 and 2E-Bulk Si (b) TO phonon modes for PS samples 2E-100, 2E-60 and 2E-Bulk Si

RSC Advances Accepted Manuscript

View Article Online
DOI: 10.1039/C3RA42205D

COMPOSITIONAL CHARACTERISATION OF METALLURGICAL GRADE SILICON AND POROUS SILCION NANOSPONGE PARTICLES, Chadwick *et al.*

Tables

Table 1 XRF and ICP concentrations of surface elements for 2E-Bulk and 2E-100

Elements	XRF (2E-Bulk) %	ICP (2E-Bulk) %	XRF (2E-100) %	(% XRF Reductions)
Fe	0.3-0.5	0.31	0.08	73-84
Al	0.08-0.2	0.18	0.038	53-81
Ca	0.03-0.08	0.031	0.014	53-83
C	<0.06	0.0327±0.0010	0	100
O	0	0.3722±0.0038	0	0

*All results were obtained in collaboration with Vesta Research

Table 2 XPS % concentrations of surface elements for 2E-100, 2E-60 and 2E-Bulk

% Concentrations	Sample 2E-100	Sample 2E-60	Sample 2E-Bulk
Fluorine	2.0	1.3	0
Carbon	28.6	24.5	8.7
Silicon	60.2	65.6	61.1
Oxygen	9.2	8.6	30.2

Published on 02 August 2013. Downloaded by University College Cork on 07/08/2013 15:02:52.

RSC Advances Accepted Manuscript

View Article Online
DOI: 10.1039/C3RA42205D

COMPOSITIONAL CHARACTERISATION OF METALLURGICAL GRADE SILICON AND POROUS SILCION NANOSPONGE PARTICLES

Edward G. Chadwick[1, 2] N.V.V. Mogili[2] Colm O'Dwyer[1,3†] Jimmy D. Moore[4], John S. Fletcher[4‡], Fathima Laffir[1] Gordon Armstrong,[1] David A. Tanner[1, 2*]

[1] Materials and Surface Science Institute, University of Limerick, Limerick, Ireland
[2] Department of Design and Manufacturing Technology, University of Limerick, Limerick, Ireland
[3] Department of Physics and Energy, University of Limerick, Limerick, Ireland
[4] School of Chemical Engineering and Analytical Science, Manchester Interdisciplinary Biocentre, University of Manchester, 131 Princess St., Manchester, M1 7DN, UK
† Present address: Department of Chemistry, University College Cork, Cork, Ireland, and Tyndall National Institute, Lee Maltings, Cork, Ireland (c.odwyer@ucc.ie)
‡ Present address: Department of Chemistry and Molecular Biology, University of Gothenburg, 41296 Gothenburg, Sweden
*E-mail: david.tanner@ul.ie, Tel: 00-353-(0)61-234130; Fax: 00-353-(0)61-202913

Published on 02 August 2013. Downloaded by University College Cork on 07/08/2013 15:02:52.

RSC Advances Accepted Manuscript

ABSTRACT

Porous silicon is generally achieved through electro-chemical etching or chemical etching of bulk silicon in hydrofluoric acid based solutions. The work presented here explores the effect of a chemical etching process on a metallurgical grade silicon powder. It is found that the metallurgical grade silicon particles contain surface bound impurities that induce a porous structure formation upon reaction with the chemical etchant applied. The correlation between the resultant porous structure formed due to the material composition is examined in detail. The elemental composition is determined using a combination of X-ray Photoelectron Spectroscopy and Time of Flight Secondary Ion Mass Spectroscopy. The porous structure is analysed using Transmission Electron Microscopy and Scanning Electron Microscopy. Three samples of the silicon particles analysed for this study include an un-etched bulk silicon powder sample and two samples of chemically etched powder. Pore formation within the particles is found to be dependent on the presence, dispersion, and local concentration of surface bound impurities within the starting powder.

Keywords: Porous Silicon, Metallurgical Grade Porous Silicon, Nanosponge

View Article Online
DOI: 10.1039/C3RA42205D

Published on 02 August 2013. Downloaded by University College Cork on 07/08/2013 15:02:52.

1. INTRODUCTION

Porous Silicon (PS) was originally discovered in 1956 by Arthur Uhlir and Ingeberg Uhlir at the Bell Laboratories in the US when electropolishing Silicon (Si) wafers using hydrofluoric acid (HF) [1]. What formed was a coloured porous film on the Si wafer with pore formation occurring in the [100] direction [2]. While this find was noted there was little interest in PS until 1990 when Canham and Lehman et al made the discovery of its room temperature photoluminescence as a result of quantum confinement effects [3-7]. There has since been an abundance of research into porous silicon and related materials [6, 8-12] to develop possible applications in areas such as optoelectronics, microelectronics, chemical and biological sensors, drug delivery devices and more recently energetic material devices [13, 14]. PS therefore has the potential for numerous applications in a variety of fields but extensive characterisation of the material is deemed essential before pursuing possible Si material applications development.

Metallurgical Grade Si (MGSi) contains a host of impurities such as Fe, Al, Ca, C and O [15-16]. These impurities are located at grain boundaries of the material when it is being manufactured [16]. Vesta Sciences have developed a process for producing low cost PS from MGSi powders through a patented chemical etching process [15, 17]. In this work, a detailed compositional investigation is carried out on this MGSi and the Metallurgical Grade Porous Silicon (MGPS) produced post-chemical etching in line with a structural characterisation of the particle porosity. The relationship between the composition of the material and the resulting porous structure formation is examined in detail in order to understand the porosity formation mechanisms of this material. It is shown that the porous morphology is that of a quantum sponge particle with Si crystallites arranged in a random porous matrix. Detailed elemental investigation links the specific composition of the PS produced from the process to the resulting mechanism of pore nucleation and

RSC Advances Accepted Manuscript

View Article Online
DOI: 10.1039/C3RA42205D

Published on 02 August 2013. Downloaded by University College Cork on 07/08/2013 15:02:52.

formation. These results provide an insight into the development of this nanosponge material when processed under such conditions. This insight can be used to help further tailor the material for various applications from biomedical engineering to military applications. Microscopical techniques including Transmission Electron Microscopy (TEM) and Convergent Beam Electron Diffraction (CBED) were applied to the material. Characteristics including pore size, volume and pore orientation are studied as an effect of the processing parameters and etching mechanism, where the elemental composition was determined using X-ray Photoelectron Spectroscopy (XPS) and Time of Flight Secondary Ion Mass Spectroscopy (TOF-SIMS). Raman spectroscopy was conducted to examine variations in crystallite structure and strain in PS arising from changes to the conditions used to prepare the PS.

2. EXPERIMENTAL

2.1 POROUS SILICON PREPARATION

The MGSi powder is supplied from Vesta Ceramics (Sweden) which is sold under the trademark of Sicomill^{TM}. The powder initially has a particle size of about 1-3mm before being jet milled. The jet milled particles are then classified into several grades with different mean particle sizes ranging from 4 microns to 11 microns. For the study here, E grade particles with a mean particle size of 4μm are used. PS particles are prepared by chemically etching the E grade MGSi particles using a patented etching process carried out by Vesta Sciences [15, 17]. The particles are chemically etched in a nitric-acid (NO_3) - (HF) based mixture as described by Farrell *et al* [15] which induces the porosity within the MGSi particles. When the etching process is complete (i.e. photoluminescence is observed due to quantum confinement of Si feature sizes below the Bohr radius of the material and also from defect induced emission for features >4-5 nm in size), the etched

RSC Advances Accepted Manuscript

View Article Online
DOI: 10.1039/C3RA42205D

Published on 02 August 2013. Downloaded by University College Cork on 07/08/2013 15:02:52.

powder is removed from the acid bath and dried in perfluoroalkoxy (PFA) trays at 80°C for 24 hours. By varying the total nitric acid concentration in the etchant mixture the surface area of these powders can also be tailored [15, 17]. The three samples of MGSi powders analysed in this paper are defined as follows ('2E' refers to a specific grade of material):

1) 2E-Bulk – The starting MGSi powder used to make the PS particles

2) 2E-100 – PS powder manufactured from the 2E-Bulk powder after chemically etching with a nitric acid concentration corresponding to that needed to obtain the highest surface area and photoluminescence (100% is defined as the nitric acid concentration that results in powders that exhibit the higher surface area, porosity and photoluminescence with an ultraviolet light [15])

3) 2E-60 – As for (2) but only chemically etched with 60% of the nitric acid used for 2E-100

2.2 HIGH RESOLUTION ELECTRON MICROSCOPY

TEM specimens were prepared by loading the PS particles onto Formvar-backed carbon-coated copper grids (Agar Scientific). TEM analysis was acquired using a JEOL JEM 2100F Field Emission Electron Microscope operating at 200kV.

TEM images were recorded with a Gatan Ultrascan 1000 digital camera for standard TEM imaging modes. The TEM is also equipped with a secondary electron imaging (SEI) detector which allows Scanning Electron Microscopy (SEM) type images to be recorded on the TEM. For CBED analysis, crystals were tilted to the [340] zone axis and a series of CBED patterns recorded in Scanning Transmission Electron Microscopy (STEM) mode with a spot size of 1.5 nm using STEM-based diffraction imaging [18].

RSC Advances Accepted Manuscript

View Article Online
DOI: 10.1039/C3RA42205D

Published on 02 August 2013. Downloaded by University College Cork on 07/08/2013 15:02:52.

2.3 TIME-OF-FLIGHT SECONDARY ION MASS SPECTROMETRY

Time of Flight Secondary Ion Mass Spectroscopy (ToF-SIMS) analysis of the 2E-bulk and etched 2E-100 Si sample was performed using the J105 3D Chemical Imager (Ionoptika Ltd UK). A layer of each sample was deposited onto a silicon substrate from a dense suspension in methanol. Images were acquired over a 500 × 500 μm^2 field of view, with a primary ion dose of 1.7×10^{13} ions/cm^2 using a 40 keV C_{60}^+ primary ion beam. Following acquisition principal components analysis (PCA) was performed on the two data sets. PCA is a multivariate technique commonly used in SIMS and is a widely used dimensionality reduction technique for data analysis and interpretation. PCA converts the data into a series of principal components (PCs). Each PC has an associated loading which is the contribution of each mass channel to that PC. Each pixel/spectrum then has a corresponding score on that loading. Principal components are ordered highest to lowest (highest being PC1) in terms of the degree of variance within the data captured by that PC.

2.4 RAMAN SCATTERING SPECTROSCOPY

Raman scattering spectra were acquired from powder dispersions of both as-received and etched MGSi particles using a Horiba Jobin Yvon Labram 1A Raman spectrometer. Spectra were collected using a 532 nm 100 mW laser source, 1800 line/mm grating and 10× objective, unless noted otherwise. The spectrometer was calibrated against the 521cm^{-1} Transverse Optical (TO) phonon frequency of a Si (100) wafer; the resolution of the spectrometer is < 2 cm^{-1}. Each spectrum presented is the average of three accumulations.

RSC Advances Accepted Manuscript

View Article Online
DOI: 10.1039/C3RA42205D

Published on 02 August 2013. Downloaded by University College Cork on 07/08/2013 15:02:52.

2.5 X-RAY PHOTOELECTRON SPECTROSCOPY

XPS was performed to analyse the surface chemistry of the Si particles using a Kratos AXIS 165 spectrometer with monochromatic Al Kα radiation of energy 1486.6 eV. High resolution spectra were taken at fixed pass energy of 20 eV. Binding energies were determined using C 1s peak at 284.8 eV as charge reference. For construction and fitting of synthetic peaks of high resolution spectra, a mixed Gaussian-Lorenzian function with a Shirley type background subtraction were used.

2.6 X-RAY FLUORESCENCE AND INDUCTIVELY COUPLED PLASMA SPECTROSCOPY

The samples were supplied with X-Ray Fluorescence (XRF) Spectroscopy and Inductively Coupled Plasma (ICP) Spectroscopy completed by Vesta Sciences as shown in section 4.1.

3. EXPERIMENTAL RESULTS AND DISCUSSION-MORPHOLOGY

3.1 SEM AND TEM OF SILICON PARTICLE SURFACE STRUCTURE

The particle morphology was studied from a series of SEM and TEM images. Figures 1a and b show high resolution SEI images of sample 2E-100. These images were acquired in SEI mode, which provided higher resolution imaging of the surface morphology compared to FESEM and thus shows the porous surface area in much more detail. On examination of the selected PS particle it is evident that the surface of the particle is completely porous in nature. The Si particle size ranges from 4 - 5 μm with pore sizes ranging from 8 - 15 nm in diameter[19]. Similar porosity was observed for sample 2E-60

RSC Advances Accepted Manuscript

View Article Online
DOI: 10.1039/C3RA42205D

but with a smaller pore volume per surface area[19]. The 2E-Bulk Si sample consists of solid Si particles[19].

Figure 1 (a) SEI micrograph of sample 2E-100 oriented in [3 4 0] zone axis (b) Corresponding higher magnified image clearly showing the porous nature of the particle

3.2 TEM-CBED OF SILICON PARTICLES

TEM-CBED analysis was performed on the surface of the 2E-Bulk sample to examine the possible strain change within the material when compared to sample 2E-100. Secondary Electron Imaging (SEI) in combination with high spatially Convergent Beam Electron Diffraction (CBED) was performed. Due to the converged beam of illumination, High Order Laue Zone (HOLZ) lines are formed inside the CBED patterns (Figure 2) and are very sensitive to any lattice changes. Based on the appearance of HOLZ lines, the qualitative nature of the pore structure was determined.

Figure 2 a) Convergent Beam Imaging (CBIM) micrograph of [340] oriented unetched Si particle exhibiting both real and reciprocal space information b) Corresponding Secondary Electron Image (SEI) of unetched Si particle illustrating the surface morphology of the crystal

Along the spectrum image line as indicated in Figure 3a for an unetched Si particle (2E-Bulk), successive [340] HOLZ lines are collected to identify any local lattice distortions. <004> two beam CBED patterns are also recorded along the spectrum image line and

Published on 02 August 2013. Downloaded by University College Cork on 07/08/2013 15:02:52.
RSC Advances Accepted Manuscript

View Article Online
DOI: 10.1039/C3RA42205D

Published on 02 August 2013. Downloaded by University College Cork on 07/08/2013 15:02:52.

based on the distance between Kossel – Möllenstedt (KM) fringes inside CBED discs, particle thickness has been calculated and shown to vary from 358 nm to 393 nm. Figure 3b and c show two experimental [340] HOLZ line patterns obtained from the spectrum image series. Figure 3d and e highlight the region where the HOLZ lines intersect showing no shift in the HOLZ lines intersection point indicating that the lattice spacing remains constant within this region.

Figure 3a) SEI image of a 2E-Bulk particle indicating the spectrum image line where sequential CBED patterns are collected b), c) Two [340] CBED patterns taken from spectrum image and HOLZ lines intersection points which are very sensitive for lattice changes are highlighted d), e) Enlarged region of [340] HOLZ lines showing that there is no shift / change in intersection point.

In the fully etched porous Si particles (2E-100), a series of [340] HOLZ line patterns were taken along the spectrum image line as seen in Figure 4a. Figures 4b and c show two different HOLZ lines patterns that were part of a spectrum imaging series clearly displaying a shift in the HOLZ line intersection positions; the shift is shown at higher magnification in Figures 4d and e. As the HOLZ lines are related to the HOLZ reflections with large reciprocal lattice vectors of the crystal lattice, their positions are highly sensitive to lattice deformations [20]. To further understand the HOLZ line shift diffraction contract imaging is performed as discussed in section 3.3

Figure 4a) High resolution SEI micrograph of sample 2E-100 PS sample showing spectrum imaging location of one particular pore b), c) Two [340] CBED patterns collected from spectrum image showing the shift of HOLZ line position d), e) Enlarged

RSC Advances Accepted Manuscript

View Article Online
DOI: 10.1039/C3RA42205D

region of [340] HOLZ lines clearly showing shift in the position of intersection point. (Reader is advised to go through the supplementary video file in order to visualise how the HOLZ lines move in the spectrum imaging patterns)

3.3 DIFFRACTION CONTRAST IMAGING OF POROUS SILCION NANOSPONGE PARTICLES

Dark field HRTEM imaging is used in a two-beam condition to obtain high contrast images of the crystalline phases. Figure 5, represents <220> dark field images obtained from (a) sample 2E-Bulk and (b) 2E-100. The required diffraction contrast was established by tilting the particles from the [011] zone axis orientation towards the (220) reflection. In Figure 5a, due to the non-uniform thickness of the Si particle in the electron beam direction, thickness fringes are observed. In Figure 5b, bright spots are observed on the particle surfaces indicating that crystalline Si nanoparticles appear on the surface after etching. These Si clusters have been etched out of the bulk Si particles and are scattered among the porous regions of the PS samples. Hence, from the dark field imaging, it is clear that Si nano-crystallites exist on the PS particle surface, so the main cause for the line-shift observed in the PS particles in section 3.2 is due to presence of Si nano-crystallites on the particle surfaces.

The analysis here corresponds to work by Peng *et al* describing the mechanism for pore formation showing metal particles at the bottom of the pores of a Si sample material after etching and pore formation [(21)]. In the case of MGPS it is proposed that the metallic impurities which are on the surface in the 2E-Bulk sample could also be driven into the Si material during pore formation leaving only the removed Si dispersed among the surface pores, confirming the relative abundance in variations between elements detected by

Published on 02 August 2013. Downloaded by University College Cork on 07/08/2013 15:02:52.

RSC Advances Accepted Manuscript

View Article Online
DOI: 10.1039/C3RA42205D

XRF, ICP and TOF-SIMS post-etching described in later sections. Si nano-particles have also been observed previously where particles were dispersed among a surface bound oxide layer post-electrochemical etching [22].

Figure 5 (a) Typical <220> dark field images of sample 2E-Bulk Si particle and (b) sample 2E-100 PS particle

4. EXPERIMENTAL RESULTS AND DISCUSSION – ELEMENTAL ANALYSIS

4.1 X-RAY FLUORESCENCE AND INDUCTIVELY COUPLED PLASMA SPECTROSCOPY OF SLICON PARTICLES

XRF and ICP analysis were carried out on samples 2E-Bulk and 2E-100 to explore the concentrations of elements present around the surface and within the Si particles. Table 1 shows the quantitative concentrations of elements detected. It was found that the Fe (0.5%) and Al (0.2) concentrations are greatest, followed by Ca (0.08%) and C (0.06%) in sample 2E-Bulk. These values indicate just how small these levels of impurities are dispersed throughout the Bulk Si particles. These values correspond to the patent standard and are also in line with what is observed for standard MGSi powder [15-16]. The levels of Fe, Al, Ca, C and O observed in sample 2E-100 using XRF analysis are less than those observed in sample 2E-Bulk. This corresponds to the mechanism that the MGSi powder contains impurities which, upon reaction with the HF based electrolyte, induce porosity at the Si particle surface via electroless etching processes. The impurities are then attacked in a cathodic reaction which leaves a porous structure throughout the outermost region of the Si particle. These impurities would then be significantly reduced in the material to smaller amounts dispersed throughout the remaining non-porous region of the PS sample. Previous reports have shown that the application of certain elements onto a Si surface will

Published on 02 August 2013. Downloaded by University College Cork on 07/08/2013 15:02:52.
RSC Advances Accepted Manuscript

View Article Online
DOI: 10.1039/C3RA42205D

Published on 02 August 2013. Downloaded by University College Cork on 07/08/2013 15:02:52.

induce porous layer formation once electro-chemically or chemically etched in a HF based solution. Metal-assisted etching using thin films of Pt and Ag on Si has shown PS formation [23-26] and incorporating Fe into HF solutions has also been shown to affect the etching process to some degree [27]. Al has already been shown to induce a porous layer structure formation in Si in a study which chemically etched a thin Al film on a Si substrate [28]. The Al film (up to 200 nm in thickness) reacted with the HF solution and in this case was the key mechanism for hole initiation and the porous structure formation [28]. These results correlate directly to the porous structure formation mechanism proposed in this paper and is further highlighted by the mass loss (% reductions) of the impurities pre and post chemical etching. Fe which is the most abundant element is reduced by 84% while Al and Ca are reduced by 81% and 83% respectively.

Table 1 XRF and ICP concentrations of surface elements for 2E-Bulk and 2E-100

4.2 X-RAY PHOTOELECTRON SPECTROSCOPY OF SILICON PARTICLES

XPS was utilised to establish the surface layer composition of the PS particles. The three samples analysed included the 2E-Bulk Si sample, sample 2E-100 and sample 2E-60. All samples showed the presence of Si, O and C and in the case of chemically etched 2E-100 and 2E-60 samples notable amounts of F were also identified. Other impurities were not observed perhaps due to their very low concentrations (less than the detection limit of XPS ~ 0.1 atomic %). Figure 6 shows the XPS survey spectra of the 2E-Bulk Si sample. The prominent peaks are Si (Si 2p, 2s), C (C 1s) and O (O 1s, KLL X-Ray induced Auger transition). These peaks are similar to previous XPS analysis of PS [29]. Feng *et al* has shown that 200 μm thick PS membranes showed similar peak positions to those observed

RSC Advances Accepted Manuscript

View Article Online
DOI: 10.1039/C3RA42205D

Published on 02 August 2013. Downloaded by University College Cork on 07/08/2013 15:02:52.

here for the PS and Si particles [29]. Quantification of elements from XPS analysis is given in Table 2 with relative percentage concentrations of F at 2%, C at 28.6%, Si at 60.2%, and O at 9.2% for 2E-100. Similar results were obtained for 2E-60. The respective peaks for 2E-Bulk Si indicated percentage concentrations C at 8.7%, Si at 61.1%, and O at 30.2%. The presence of F in the PS samples can be attributed to the etching process.

Figure 6 a) XPS analysis of sample 2E-Bulk; b) and c) High resolution Si 2p spectra of 2E-Bulk and 2E-60 respectively.

A high resolution Si 2p spectrum from the 2E-Bulk Si sample is shown in Figure 6b and can be fitted with three sets of doublets. The majority of silicon is present as elemental Si with Si $2p_{3/2}$ at a binding energy of 98.8 eV. The peaks at higher binding energy of 101.1 eV and 102.8 eV can be attributed to silicon oxide SiO_x ($x < 2$) and SiO_2 respectively [30-31]. The presence of the related O 1s at 532.3 eV confirms that the more abundant of the oxides, SiO_2, is largely stoichiometric. However, Si 2p spectra of sample 2E-60 (Figure 6c) are dominated by low binding energy peaks corresponding to elemental silicon with a relatively minor contribution from higher binding energy components at 103.6 eV which may be attributed to SiO_2 or a residual SiF_x complex from the etching process, which proceeds according to a series of galvanic displacement reactions according to

$M^+ + e^- \rightarrow M^0$ (where M is the metal impurity)

$Si + 2H_2O \rightarrow SiO_2 + 4H^+ + 4e^-$

$SiO_2 + 2HF_2^- + 2HF \rightarrow SiF_6^{2-} + 2H_2O$

The higher content of oxygen on the surface of sample 2E-Bulk (30.2 atomic %) can be attributed to it being the bulk starting material and likely to have undergone surface oxidation. The O content is significantly reduced in the PS samples indicating it was

RSC Advances Accepted Manuscript

View Article Online
DOI: 10.1039/C3RA42205D

Published on 02 August 2013. Downloaded by University College Cork on 07/08/2013 15:02:52.

removed through the applied chemical etching process and HF reaction at the Si surface. Increased carbon content on the surface of the etched PS is due to the environment in which XPS analysis is conducted.

Table 2 XPS % concentrations of surface elements for 2E-100, 2E-60 and 2E-Bulk

4.1 TIME OF FLIGHT SECONDARY ION MASS SPECTROSCOPY OF SILICON PARTICLES

Further analysis of the Si particle composition was carried out using TOF-SIMS analysis. Sample 2E-Bulk showed the standard elements associated with the MGSi powder. The total ion images of both the bulk and etched samples can be seen in Figure 7. Images were acquired over a $500 \times 500\ \mu m^2$ field of view, with a primary ion dose of 1.7×10^{13} ions/cm^2 using a 40 keV C_{60}^+ primary ion beam.

Figure 7 Total ion images ($500 \times 500\ \mu m^2$) of (a) 2E-Bulk sample (b) 2E-100 particles.

The scores and loadings for the Principal Component (PC) 2 of the 2E-bulk un-etched particles can be seen in the spatial score maps in Figure 8a. The scores image (Figure 8a) highlights where red indicates a negative score and green indicates a positive score. In comparison to the total ion image (Figure 7a) it is apparent that the highlighted regions with this chemistry i.e. green regions are cluster/groups of the Si particles. From the corresponding loadings (Figure 8b) it is evident that the Al^+, Ca^+ and Fe^+ are correlated to these Si cluster groups, confirming the elemental composition analysis from XRF and ICP analysis in Table 1. Some salts (Na^+, K^+) are also correlated in this PC.

RSC Advances Accepted Manuscript

View Article Online
DOI: 10.1039/C3RA42205D

Published on 02 August 2013. Downloaded by University College Cork on 07/08/2013 15:02:52.

The etched samples (2E-100) can be considered in a similar manner. The scoring map indicates a reduced abundance of the Al^+, Ca^+ and Fe^+ species, captured in the PC3 loading in Figure 8d. These analyses have demonstrated the presence of these metals on the Si particles before and after etching and are thus not released into the etching solution after chemical reduction during the etching process. Remnant Na^+, K^+ were easily dissolved and removed from the particles in the aqueous HF-based etching solution. However, changes in the valence or quantitative relative abundances cannot be deciphered from this analysis, particularly since the presence of reduced metal species after galvanic displacement or electroless reactions are lodged within the nanoporous structure of the silicon sponge particles.

Figure 8 (a, b) Scores image and the corresponding TOF-SIMS loading spectrum from PC2 of the 2E-Bulk Si particles and (c, d) from PC3 of the etched 2E-100 Si particles.

4.2 RAMAN SCATTERING SPECTROSCOPY OF POROUS SILICON QUANTUM SPONGE PARTICLES

Raman Spectroscopy is a powerful technique that can be employed in structural and dynamic studies of PS [29, 32]. A typical Raman Spectrum for crystalline Si usually consists of a symmetric first order transverse optical phonon centred at ~521cm^{-1} [33-34]. As the grain size in micro-crystalline Si decreases, the Raman shift and peak width increases and the line-shape becomes asymmetric (which also occurs with doping changes, which is invariant in this case) with an extended tail at lower frequencies for quantum confinement or small size effects. In amorphous Si the Raman peak is broad and usually weak at 480 cm^{-1} [33-34]. Here, micro-Raman scattering spectroscopy was conducted on samples 2E-100, 2E-60 and 2E-Bulk Si (Figure 9a) to examine the development and influence of

RSC Advances Accepted Manuscript

View Article Online
DOI: 10.1039/C3RA42205D

Published on 02 August 2013. Downloaded by University College Cork on 07/08/2013 15:02:52.

porosity on the overall structure, specifically the presence and associated influence of nano-sized crystallites of silicon.

The main Si peak in the 2E-Bulk Si occurs at 517cm^{-1}, compared to 521cm^{-1} measured for bulk Si(100) and the TO phonon mode is sharp and symmetric compared to highly doped Si(100), which displays a blue asymmetry indicative of highly p-type Si. The TO modes for both 2E-60 and 2E-100 occur at 516cm^{-1} and 510cm^{-1}(Figure 9b), has an asymmetric line shape with asymmetry appearing on the lower (red) energy side indicative of phonon confinement due to reduced sizes, as the doping density remains invariant for the same particles and no excess heating has been applied externally or through Jourle heating by the incident Raman probe beam. Generally for PS it is considered that the broadening and a downshift of the TO mode towards lower energies indicates the presence of nanoscale features of the crystalline structures and is distinct for high porosity layers of PS [35]. A slight lower energy downshift of the peaks was observed in 2E-100 compared to 2E-Bulk Si. These quantum confined features come from the smallest pore wall structures but particularly from the high density of small <5 nm crystallites seen by STEM, as outlined in section 3.3. These core Si values do not correlate directly with Si or PS substrates with typical Raman peaks around 521cm^{-1} but are more closely linked to the PS membranes studied by Feng *et al* [29] . In that work, Raman spectra of PS membranes removed from anodically oxidised p-type <100> Si substrates, showed dominant Raman shifts between 502 and 512 cm^{-1} [29]. The bands located near 300 cm^{-1} correspond to an acoustic phonon (2TA). These values correlate directly to what is observed for sample 2E-100 in Figure 9. The features between 900-1000 cm^{-1} indicate second order optical modes [29], as seen in both samples 2E-100 and 2E-60.

It has also been shown that surface strain or stress in PS can also contribute to a downshift in the Raman peak as is observed from 2E-Bulk Si to 2E-100 in Figure 9b. The

RSC Advances Accepted Manuscript

View Article Online
DOI: 10.1039/C3RA42205D

Published on 02 August 2013. Downloaded by University College Cork on 07/08/2013 15:02:52.

positions of the characteristic Raman peaks of a material correspond to the vibrational energy of the phonon modes. However, if the crystal lattice deforms, the position of the mode may shift to the left or to the right, due to an energy variation in the vibration of the lattice. Lang *et al* reports that the lattice constant of PS is somewhat strained and a stress value corresponding to such a lattice strain is known to shift the Raman peak to lower energies [(36)] known as phonon softening. The incorporation of a surface oxide may relax the surface strain to some degree in PS [(36)]. The Authors discuss a linear relationship between uniaxial or biaxial stress and the shift of the TO mode of the sample. The reduction in total free energy within the particle, is such that the porous particle is rendered more brittle compared to the bulk particle can be calculated from the empirical formula [(37)] $\varepsilon = \sigma_{st} \cdot \Delta\omega$, where ω represents the peak positions in cm^{-1} for strained and bulk Si, and $\Delta\omega$ represents (ω_{bulk} - ω_{pore}), $\sigma_{st} = 0.123$ is the inverse strain-phonon coefficient in cm, and ε is the % strain.

The quantum confinement caused by crystallites of silicon and also the smallest of porous wall features by monitoring the asymmetry and frequency shift or the TO phonon mode is shown in Figure 9b. For both 2E-bulk and 2E-100 samples, the Raman shift from respective TO modes correlates to a % free energy reduction of 47% for 2E-bulk particles compared to a Si (100) crystal, and a further 18% reduction (65% compared to Si(100)) upon partial porosification for 2E-60 samples, but a very large 136% reduction in free energy for fully etched 2E-100 particles compared to Si(100). In this process, every stress relieving interface will most likely contain metallic ions amenable to electroless etching and thus all galvanic displacement reactions on the surface will lead to a significant reduction in internal particle free energy.

RSC Advances Accepted Manuscript

View Article Online
DOI: 10.1039/C3RA42205D

Figure 9 (a) Micro-Raman Spectrum of PS samples 2E-100, 2E-60 and 2E-Bulk Si (b) TO phonon modes for PS samples 2E-100, 2E-60 and 2E-Bulk Si

The crystallite size *L* of the porous Si quantum sponge particles can be estimated from the Raman shift according to:

$$\Delta\omega = 52.3\ (0.543/L)^{\alpha}$$

where $\Delta\omega$ is the Raman shift between that from a silicon wafer (521 cm^{-1}) and the TO phonon frequency from each of the TO phonon peaks from the Si sponge particles. The power law dependence determined empirically is $\alpha = 1.59$. The crystallite sizes for 2E-60 and 2E-100 (with respect to a Si wafer) are estimated to be 1.93 and 1.16 nm respectively. These values correspond to the electron microscopy observations in Section 3.3.

5. DISCUSSION – POROSITY FORMATION

5.1 POROSITY FORMATION IN METALLURGICAL GRADE SILICON

Understanding the porosity formation mechanisms in Si, when processed under certain conditions is essential for successful tailoring of the material for final applications. Hence there has been an abundance of work completed on different Si materials using different etching methods [38-41]. PS is generally achieved when doped Si wafers are electrochemically or chemically etched using HF based solutions [42, 43]. Pore formation and propagation is usually dependant on the crystallographic orientation of the Si wafers used in an electrochemical or chemical etching process. Other important properties of the PS material such as resultant pore size, pore volume and pore depth are very much

Published on 02 August 2013. Downloaded by University College Cork on 07/08/2013 15:02:52.

RSC Advances Accepted Manuscript

View Article Online
DOI: 10.1039/C3RA42205D

Published on 02 August 2013. Downloaded by University College Cork on 07/08/2013 15:02:52.

dependant on the anodisation conditions applied *i.e.* HF concentration, oxidation, carrier type (n-type or p-type), current density applied, the anodisation method and duration etc [8-10, 44-45]. These parameters can be tuned to some degree resulting in tailoring of the Si porosity to desired conditions. Other etching methods derived from standard electrochemical and chemical etching processes include metal-assisted etching and in this method, PS is produced by electroless etching and galvanic displacement reactions between certain metallic ions at the surface in a fluoride-containing electrolyte [23-26]. The application of a thin metallic film or metal particles (Au, Pt, Al, Ag, Palladium (Pd)) onto the surface of the Si substrate results in a cathodic-anodic reaction (metal film or particle being the cathode) and the Si material (when oxidised becoming the anode) which then results in a boring or sinking of the metal particles into the Si surface creating pore formation. Various metallic-Si interface reactions can be explained but essentially in the case of Ag particles for example, the Si beneath the Ag is oxidised by hole injection when the oxidising agent (hydrogen peroxide (H_2O_2), sodium persulfate ($Na_2S_2O_8$) or HNO_3 are typically used in the etching solution) is reduced on the Ag. Therefore the Si is oxidised which reacts with the HF to form a water-soluble complex and thus the holes are then simply the sinking or boring tracks of the Ag particles [24]. Etching pure Si wafers in HF without prior hole injection simply results in a passivated surface layer [46]. Understanding these porosity formation mechanisms is key in outlining the mechanisms responsible for porosity formation in MGSi containing metallic impurities, processed under similar conditions.

XRF and ICP analysis confirmed the presence of Fe, Al, Ca, C and O dispersed throughout the MGSi particles. These metal ions which are considered mostly surface bound within the Si particles react with the HF based chemical etchant applied, which in

RSC Advances Accepted Manuscript

View Article Online
DOI: 10.1039/C3RA42205D

Published on 02 August 2013. Downloaded by University College Cork on 07/08/2013 15:02:52.

the case of this study is HF, HNO_3 and water (H_2O). Nitric Oxide (NO) is produced on the surface of the Si which serves as the hole injector [44]. The rate of dissolution depends on the number of injected holes per atom, which in the present case is greatest for Al^{3+} compared to Fe^{2+} or Ca^{+}. Beck and Gerischer proved that the reaction rate is proportional to the surface concentration of holes [47]. Due to the different reactivities of surface electrons and holes, the doping type of the crystal leads to very different reactivites for *n*-type and *p*-type doping; in the case of intrinsically doped MGSi particles here, the role of the hole injector ions is paramount.

The presence of a hole in the valence band reduces the strength of bonds in the vicinity and makes the substrate atoms more susceptible to attack by nucleophiles. Similarly, the presence of a conduction band electron weakens bonds in its vicinity and makes those substrate atoms susceptible to electrophilic attack. Additionally, the likelihood for these galvanic displacement reactions also depends on having a small electronegativity difference between the metal ion and the silicon and coupled with the relative abundance of the respective ions, leads to variable etching rates. All three will participate and their spatial density on the particle (highest on the surfaces which were originally the grain boundaries in the pre-milled MGSi) results in a complicated process where the result is a Si 'sponge'. It is noted that the Si 'sponge' still contains some levels of impurities which are greatly reduced as determined using XRF and ICP. The TOF-SIMS spectra correlate well with the XRF and ICP analyses when the galvanic displacement reactions are considered. Each of the metal ions is reduced by extracting a number of electrons from the silicon equivalent to the valence of the ion; the rate of electroless etching is greatest for Al and thus the relative abundance is minimum post-etching as the metallic Al^0 is contained furthest into the sponge structure (assuming some of each element is lost through equivalent mass transport into the aqueous etching solution). This etching process

RSC Advances Accepted Manuscript

View Article Online
DOI: 10.1039/C3RA42205D

Published on 02 August 2013. Downloaded by University College Cork on 07/08/2013 15:02:52.

also has a resultant effect in that Si remnants are removed during the etching process and are then dispersed among the surface pores as nano-crystallites. This is observed through TEM-CBED and Diffraction contrast imaging of the PS particles and confirms the relative abundance in variations between elements detected by XRF, ICP and TOF-SIMS post-etching. Raman Spectroscopy confirmed these Si nano-crystallites result in a lower energy downshift of the peaks as observed in 2E-100 compared to 2E-Bulk Si and the calculated crystallite size conforms to what is observed through Diffraction contrast imaging. The Raman data points to a reduction in free energy within the samples after etching, which may indicate strain relaxation within individual particles as a result of the reduction of impurity levels.

While random levels of impurities resulting in random pore formation at different sites is also possible the majority of pores will be formed at the outermost surface resulting in a PS shell or sponge surrounding a solid Si core. In the case of sample 2E-100 which has an average particle size of about 4-5μm then this porous outer shell can be up to 1μm thick as observed through FIB and SEM [19, 48]. In sample 2E-60 a similar pattern structure is observed but the porous outer shell is ~ 600 nm thick for the same sized particles as sample 2E-100 [19, 48]. This is due to the time difference in the etching processes. Secondary electrons (SE) are those electrons emitted by the specimen which are having energies in the range of 0 to 50 eV. Due to these weak energies of SE, they are limited to very small depth called escape depth below the surface of the particle [49]. Hence Secondary Electron Imaging (SEI) is highly dependent on surface topography of the material.

RSC Advances Accepted Manuscript

View Article Online
DOI: 10.1039/C3RA42205D

Published on 02 August 2013. Downloaded by University College Cork on 07/08/2013 15:02:52.

6. CONCLUSIONS

The porous silicon (PS) used in this study is comprised of metallurgical grade PS particles that contain a porous sponge-like boundary up to 1μm thick with a solid silicon core as a result of the etching process. CBED analysis on individual particles has indicated no shift in HOLZ Lines when different areas of the particles of the as-received unetched material is analysed. Shifts in these HOLZ lines occur on etched samples, but diffraction contrast imaging indicates the presence of small crystallites (~1nm) on the surface of etched particles which are likely to have led to the HOLZ line shifts. The discovery of these small crystallites etched from the pores of the Si particles has not previously been reported in these materials, but is backed up in this paper through micro Raman measurements.

XPS, ICP and XRF data confirms the presence of impurities in the Si particles analysed, while the TOF-SIMS data gives a map of the elemental distributions which has not been observed previously. It is clear that the porosity formation mechanisms for MGSi when chemically etched using the method outlined previously is due to the galvanic displacement reactions between the metal ions (impurities) at the surface of the MGSi particles and the chemical etchant composition used. The Raman data highlights a free energy reduction in the samples post-chemical etching, which may indicate strain relaxation within individual particles due to the reduction of impurity levels.

RSC Advances Accepted Manuscript

ACKNOWLEDGEMENTS

The Authors would like to acknowledge the financial support of Enterprise Ireland, Vesta Sciences (EI IP 2007 0380 Vesta/ UL) and PRTLI cycle 4. The support of Vesta Sciences and Dr Shanti Subramanian for providing PS samples, XRF and ICP data. The authors

View Article Online
DOI: 10.1039/C3RA42205D

would also like to thank Paula Olsthoorn, Gaye Hanrahan, Calum Dickinson, Wynette Redington, and Shohei Nakahara for analytical results and useful discussion.

Published on 02 August 2013. Downloaded by University College Cork on 07/08/2013 15:02:52.

RSC Advances Accepted Manuscript

View Article Online
DOI: 10.1039/C3RA42205D

Published on 02 August 2013. Downloaded by University College Cork on 07/08/2013 15:02:52.

REFERENCES

1. A. Uhlir, "Electrolytic shaping of germanium and silicon", Bell Syst. Tech. J., vol. 35, 1956, pp. 333–347.
2. Xifré Pérez, E., Design, fabrication and characterization of porous silicon multilayer optical devices. 2007.
3. Guerrero-Lemus, R., F. A. Ben-Hander, J. L. G. Fierro, C. Hernández-Rodríguez, and a.J.M. Martínez-Duart, Compositional and photoluminescent properties of anodically and stain etched porous silicon. phys. stat. sol. (a), 2003. **197**: p. 137–143.
4. Canham, L.T., Silicon quantum wire array fabrication by electrochemical and chemical dissolution of wafers. Applied Physics Letters, 1990. **57**: p. 1046.
5. Parkhutik, V., Analysis of Publications on Porous Silicon: From Photoluminescence to Biology. Journal of Porous Materials, 2000. **7**(1): p. 363-366.
6. V. Lehman, H.F., Formation Mechanism and Properties of Electrochemically Etched Trenches in n-Type Silicon. J. Electrochem. Soc., 1990. **137** (2): p. 653-659.
7. V. Lehman, U.G., Porous silicon formation: A quantum wire effect. Appl. Phys. Lett. ,1991. **58**: p. 856.
8. O'Dwyer, C., Buckley, D.N., Sutton, D., Newcomb, S.B., J. Electrochem. Soc. Anodic Formation and Characterization of Nanoporous InP in Aqueous KOH Electrolytes, 2006. **153**(12): p. G1039-G1046.
9. O'Dwyer, C., Buckley, D.N., Sutton, D, Serantoni, M., Newcomb, S.B., An Investigation by AFM and TEM of the Mechanism of Anodic Formation of Nanoporosity in n-InP in KOH. J. Electrochem. Soc., 2007. **154**(2): p. H78-H85.
10. O'Dwyer, C., Buckley, D.N., Newcomb, S.B., Langmuir, 21, 8090 (2005), Simultaneous Observation of Current Oscillations and Porous Film Growth during Anodization of InP. Langmuir, 2005. **21**: p. 8090-8095.
11. V. Lehman, "Electrochemistry of Silicon", Wiley-VCH, Weinhem, 2002
12. M. J. Sailor, "Porous Silicon in Practice. Preparation, Characterization and Applications", Wiley-VCH, Weinhem, 2011
13. Becker, C., Currano, L., Churaman, W., Characterization and Improvements to Porous Silicon Processing for Nanoenergetics. Storming Media-Pentagon Reports, 2008: p. 20.
14. Anglin, E.J., Porous silicon in drug delivery devices and materials. Advanced Drug Delivery Reviews, 2008. **60**(11): p. 1266-1277.
15. Subramanian, S., Limaye, S.Y., Farrell, D., 2006 Silicon Nanosponge Particles. Ireland Patent WO/2006/121870, 16 November 2006.
16. Kareh, K., Ghahremaninezhad, A., Asselin, E., Electrochemical properties of metallurgical-grade silicon in hydrochloric acid. Electrochimica Acta, 2009. **54**(26): p. 6548-6553.
17. Subramanian, S., Tiegs, T., Limaye, S., (2008) Paper presented at the proceedings of the Army Science Conference, Orlando, 1-4 December 2008
18. Watanabe, M., Microsc. Microanal., . (2007)(13,): p. 962-963,.
19. Chadwick, E., S. Beloshapkin, and D.A. Tanner, Microstructural Characterisation of Metallurgical Grade Porous Silicon Nanosponge Particles. Journal of Materials Science, 2012.
20. De Graef, M., Introduction to Conventional Transmission Electron Microscopy. 2003: Cambridge University Press
21. Peng, K., Motility of Metal Nanoparticles in Silicon and Induced Anisotropic Silicon Etching. Advanced Functional Materials, 2008. **18**(19): p. 3026-3035.

RSC Advances Accepted Manuscript

View Article Online
DOI: 10.1039/C3RA42205D

Published on 02 August 2013. Downloaded by University College Cork on 07/08/2013 15:02:52.

22. Sorokin, L.M., Structural and electrophysical properties of a nanocomposite based upon the Si-SiO_2 system. Microscopy of Semi-conducting materials.
23. Chattopadhyay, S., X. Li, Bohn, P.W., In-plane control of morphology and tunable photoluminescence in porous silicon produced by metal-assisted electroless chemical etching. Journal of Applied Physics, 2002. **91**(9): p. 6134-6140.
24. Douani, R., Formation of aligned silicon-nanowire on silicon in aqueous HF/(AgNO3 + Na2S2O8) solution. Applied Surface Science, 2008. **254**(22): p. 7219-7222.
25. Yae, S., Formation of porous silicon by metal particle enhanced chemical etching in HF solution and its application for efficient solar cells. Electrochemistry Communications, 2003. **5**(8): p. 632-636.
26. Megouda, N., Au-assisted electroless etching of silicon in aqueous HF/H2O2 solution. Applied Surface Science, 2009. **255**(12): p. 6210-6216.
27. Solomon, I., Intense photoluminescence of thin films of porous hydrogenated microcrystalline silicon. Journal of Applied Physics, 2008. **103**(8): p. 083108-083108-4.
28. Dimova-Malinovska, D., Preparation of thin porous silicon layers by stain etching. Thin Solid Films, 1997. **297**(1-2): p. 9-12.
29. Feng, Z.C., Wee, A.T.S., Multi-Technique study of porous silicon membranes by Raman Scattering, FTIR, XPS, AES, and SIMS, in POROUS SILICON, R.T. Z C Feng, Editor. 1994. p. pp 175-194.
30. Moulder, J. F., W.F.S., Sobol, P. E., Bomben, K. D., Handbook of X-Ray Photoelectron Spectroscopy. Perkin-Elmer Corporation Physical Electronics Division. 1992.
31. v. h. s. n. g. x. NIST-XPS database.
32. Abramof, P.G., Investigation of nanostructured porous silicon by Raman spectroscopy and atomic force microscopy. Journal of Non-Crystalline Solids, 2004. **338-340**(0): p. 139-142
33. Ohmukai, M., The effects of chemical etching of porous silicon on Raman spectra. Czechoslovak Journal of Physics, 2004. **54**(7): p. 781-784.
34. Zhifeng Sui, P.P.L., Irving P., Raman analysis of light-emitting porous silicon. 1992;
35. Dubey, R. S., Gautam, D. K., Synthesis and Characterization of Nanocrystalline Porous Silicon Layer for Solar Cells Applications Journal of Optoelectronic and Biomedical Materials 2009. **Volume 1**(Issue 1): p. p. 8-1.
36. Kozlowski, F., P.S., Lang, W., Micro Raman Investigations and a Structure Model for Electroluminescent Porous n-Silicon, in Porous Silicon. 1994. p. pp 149-171.
37. Tsang, J.C., P.M.M., F. Dacol, J.O. Chu, , J. Appl. Phys., 1994. **75**(8098).
38. Kolasinski, K. W. Silicon nanostructures from electroless electrochemical etching Curr. Opin. Solid State Mater. Sci. 2005
39. M.I.J. Beale, J.D. Benjamin, M.J. Uren, N.G. Chew, A.G. Cullis An experimental and theoretical study of the formation and microstructure of porous silicon, Journal of Crystal Growth, 1985
40. Oskam, G.Long, J. G. Natarajan, A. Searson, P. C Electrochemical deposition of metals onto silicon, 1997

RSC Advances Accepted Manuscript

View Article Online
DOI: 10.1039/C3RA42205D

Published on 02 August 2013. Downloaded by University College Cork on 07/08/2013 15:02:52.

41. R. L. Smith and S. D. Collins Porous silicon formation mechanisms J. Appl. Phys. 71, R1 (1992);
42. Halimaoui, A., Porous Silicon Formation by Anodisation, in Properties of Porous Silicon, L. Canham, Editor. 1997, INSPEC-The Institution of Electrical Engineers. p. 12-22.
43. Coffer, J.L., Porous Silicon Formation by Stain Etching, in Properties of Porous Silicon, L. Canham, Editor. 1997, INSPEC-The Institution of Electrical Engineers. p. 23-29.
44. Canham, L., Properties of Porous Silicon. 1997: INSPEC-The Institution of Electrical Engineers.
45. Bisi, O., Ossicini, S., Pavesi, L., Porous silicon: a quantum sponge structure for silicon based optoelectronics. Surface Science Reports, 2000. **38**(1-3): p. 1-126.
46. Gosele, U. Lehmann, V., Porous silicon quantum sponge structures: Formation mechanism, preperation methods and some properties, in Porous Silicon, Z.C. Feng and R. Tsu, Editors. 1995, World Scientific Publishing Co: New York. p. 17-39.
47. Beck, F., Gerischer, H., Redoxvorgänge an Germanium-Elektroden. Zeitschrift für Elektrochemie, Berichte der Bunsengesellschaft für physikalische Chemie, 1959. **63**(8): p. 943-950.
48. Chadwick, E.G., Tanner, D.A., Beloshapkin, S., Zhang, H., Behan, G., High Resolution Microscopical Analysis of Metallurgical Grade Nanoporous Silicon Particles, NUI Galway-UL Alliance First Annual Engineering and Informatics Research Conference, National University of Ireland, 2011.
49. Egerton, R.F., Physical principles of Electron Microscopy, 2005.

FIGURE CAPTIONS

Figure 1 (a) SEI micrograph of sample 2E-100 oriented in [3 4 0] zone axis (b) Corresponding higher magnified image clearly showing porous nature of the particle

Figure 2 a) Convergent Beam Imaging (CBIM) micrograph of [340] oriented unetched Si particle exhibiting both real and reciprocal space information b) Corresponding Secondary Electron Image (SEI) of unetched Si particle illustrating the surface morphology of the crystal

Figure 3a) SEI image of a 2E-Bulk particle indicating the spectrum image line where sequential CBED patterns are collected b), c) Two [340] CBED patterns taken from spectrum image and HOLZ lines intersection points which are very sensitive for lattice changes are highlighted d), e) Enlarged region of [340] HOLZ lines showing that there is no shift / change in intersection point.

Figure 4a) High resolution SEI micrograph of sample 2E-100 PS sample showing spectrum imaging location of one particular pore b), c) Two [340] CBED patterns collected from

RSC Advances Accepted Manuscript

View Article Online
DOI: 10.1039/C3RA42205D

spectrum image showing the shift of HOLZ line position d), e) Enlarged region of [340] HOLZ lines clearly showing shift in the position of intersection point. (Reader is advised to go through the supplementary video file in order to visualise how the HOLZ lines move in the spectrum imaging patterns)

Figure 5 (a) Typical <220> dark field images of sample 2E-Bulk Si particle and (b) sample 2E-100 PS particle

Figure 6 a) XPS analysis of sample 2E-Bulk; b) and c) High resolution Si 2p spectra of 2E-Bulk and 2E-60 respectively.

Figure 7 Total ion images (500 × 500 μm^2) of (a) 2E-Bulk sample (b) 2E-100 particles.

Figure 8 (a, b) Scores image and the corresponding TOF-SIMS loading spectrum from PC2 of the 2E-Bulk Si particles and (c, d) from PC3 of the etched 2E-100 Si particles.

Figure 9 (a) Micro-Raman Spectrum of PS samples 2E-100, 2E-60 and 2E-Bulk Si (b) TO phonon modes for PS samples 2E-100, 2E-60 and 2E-Bulk Si

LIST OF TABLES

Table 1 XRF and ICP concentrations of surface elements for 2E-Bulk and 2E-100

Table 2 XPS % concentrations of surface elements for 2E-100, 2E-60 and 2E-Bulk

Published on 02 August 2013. Downloaded by University College Cork on 07/08/2013 15:02:52.

RSC Advances Accepted Manuscript